Supporting Information

Closing the Mediterranean Marine Floating Plastic Mass Budget: Inverse Modelling of Sources and Sinks

Mikael L. A. Kaandorp,* Henk A. Dijkstra, and Erik van Sebille

Institute for Marine and Atmospheric research Utrecht, Utrecht University

E-mail: m.l.a.kaandorp@uu.nl

Number of pages: 22
Number of figures: 8
Number of tables: 2

S1: Measurement corrections and variance

Before using the plastic concentration measurements, they are corrected for vertical mixing using the correction factor introduced by Kukulka et al.[1]:

$$\frac{N}{N_{tow}} = \frac{1}{1 - e^{-\frac{dW_b}{A_0}}}, \tag{1}$$

where N_{tow} is the amount of plastics measured by the net tow, N is the corrected amount of plastic particles, d is the submerged net depth, W_b is the rise velocity of the plastic particles, and A_0 is a parameter defining the near-surface turbulence. The value for d was not provided for all references used here. Where possible, it was calculated by comparing measurements in terms of volume with measurements in terms of area. Otherwise the most commonly occurring values in the data-set were used, which is $d = 0.1$ m for nets with a height of 0.2 m, and $d = 0.15$ m for nets with a height larger than 0.2 m. The value for W_b was set to 0.0053 m/s, the median rise velocity of plastic particles found in Reisser et al.[2]. Finally, A_0 is given by

$$A_0 = 1.5 u_{*w} \kappa H_s, \tag{2}$$

where u_{*w} is estimated to be 0.0012 times the wind velocity at 10 meters (U_{10}) as given by Pugh[3], with U_{10} as obtained from wave watch III data[4]; κ is the von Karman constant with a value of 0.4; and H_s is the significant wave height. The significant wave height was estimated from U_{10} by using the relation from Rossby and Montgomery[5].

Here we use a tool from spatial statistics called the variogram, in order to assess the variance γ of plastic measurements separated by a given spatial lag distance h. This can be used to estimate the amount of subgrid scale variance which can not be captured by the model. By assessing the variance of the plastic measurements below these scales, an indication can be obtained of the maximum achievable accuracy. The variogram is calculated only for samples which were taken within a day of each other, since this is the temporal resolution of the Lagrangian model output. Since sample information is not available at every

location, an empirical variogram is constructed, considering the variance of measurements z separated by a certain distance $h \pm \delta$. The variance for the samples within this separation distance is then calculated using:

$$\gamma(h \pm \delta) = \frac{1}{2N(h \pm \delta)} \sum_{(i,j) \in N(h \pm \delta)} (z_i - z_j)^2, \tag{3}$$

where $N(h \pm \delta)$ denotes the amount of samples in a given separation distance bin. The variogram can be calculated for both the plastic abundance and mass. Results are shown in Figure S1. The samples for $\gamma(h \pm \delta)$ are colored by the amount of data point pairs used for the calculations in this figure. A Gaussian variogram was fitted through the points to show the trends more clearly. Several important observations can be made. For both types of measurements there seems to be a clear increase in the beginning, until about 20 to 40 kilometers. Afterwards this increasing trend seems to level off, although this is difficult to be certain about since there is a lack of data points for larger lag distances h, which also shows in the larger spread for $\gamma(h \pm \delta)$. What is also important to notice, is that the variance at a given lag distance is larger for the mass measurements compared to the abundance measurements. This means that more variance is expected when comparing the model to the measurements in terms of mass, and that it is more difficult to obtain information from the individual mass measurements compared to the abundance measurements for the inverse modelling process.

S2: Beaching time scale estimate

In order to get a feeling for possible parameter values of τ_{beach}, a beaching analysis was done for a set of drifters in the Mediterranean.[6] A total of 1682 drifters were analysed, to see how long these drifters in general spend time near the coast before ending up on the beach. The mesh used for the currents has a spacing of $1/16°$, corresponding to roughly 6.9 km for the Mediterranean. This distance was used to define whether a buoy is close to the coast. For

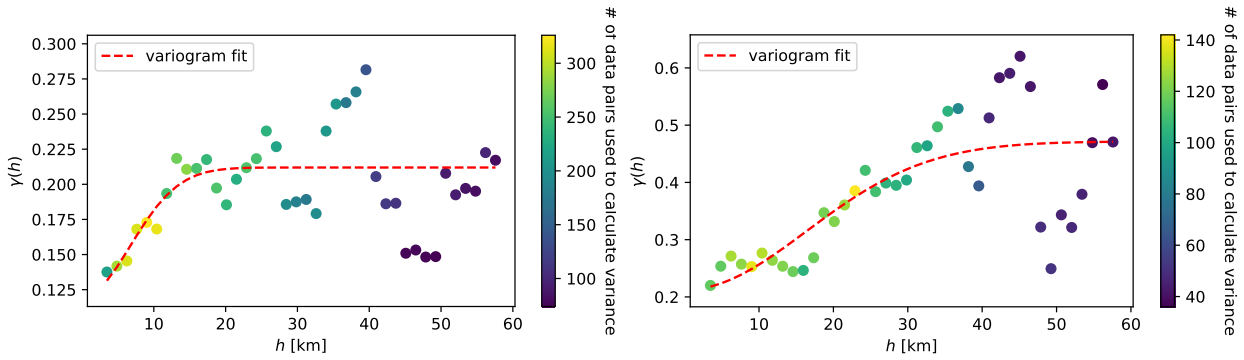

(a) plastic abundance

(b) plastic mass

Figure S1: Variograms constructed from the available plastic measurements

each buoy the time it spend near the coast was tracked: the coastal time was binned, and for each interval the fraction was calculated of the buoys not having beached. A drifter was assumed to have beached, when at its end-of-life one of the four cells surrounding the drifter had a positive elevation. A 30 arc-second bathymetry dataset was used for this[7]. Out of all buoys, 195 buoys were estimated to have beached at the end-of-life.

This analysis of drifters doesn't have to reflect the behaviour of plastic particles near the coast accurately. First of all, the particles have very different sizes, shapes, and properties. Some of the drifters are drogued, and will therefore be less sensitive to e.g. wave action and windage compared to floating plastic particles. Secondly, the beaching time scale τ_{beach} will implicitly have to take in account the recapturing of plastic particles by the water, i.e. it should be interpreted more as a time scale at which plastic particles remain permanently buried in the sand. The buoy trajectory dataset was designed to cut off when the buoy was estimated to be beached; this means that the time scale calculated from this data set should only account for one beaching event.

From the drifter buoy analysis, it followed that for each day spend near the coast, the drifter buoys have a probability of beaching of 1.2%. This translates into a time scale τ_{beach} of roughly 76 days, when assuming this probability remains constant when spending time near the coast. Since the drifter data set is sparse especially for longer coastal times, this is only a very first order estimate. For the inverse modelling step of the floating plastics,

the prior for τ_{beach} was centred at 10^2 days which is close to the buoy estimate. The inverse modelling was done on $\log_{10}$ of the values in order to span multiple orders of magnitude, with the bounds on the prior (99.7th percentile) ranging from 1 (10^1 days) to 3 (10^3 days).

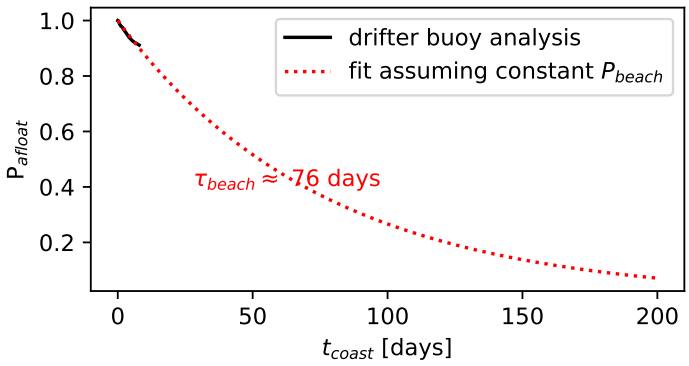

Figure S2: Beaching time scale τ_{beach} estimated from drifter buoy data

S3: Inverse modelling implementation

The most likely values for the parameters are estimated by solving a minimization problem. The cost function can be minimized by linearising the forward model around an estimate for the parameters $\mathbf{m}$, and iteratively updating the parameters using e.g. a gradient descent algorithm. The update steps were done by using a quasi-Newton method (see Tarantola [8]):

$$\mathbf{m}_{n+1} = \mathbf{m}_n - \mu_n \left(\mathbf{G}_n^T \mathbf{C}_D^{-1} \mathbf{G}_n + \mathbf{C}_M^{-1}\right)^{-1} \left(\mathbf{G}_n^T \mathbf{C}_D^{-1} (\mathbf{d}_n - \mathbf{d}_{obs}) + \mathbf{C}_M^{-1} (\mathbf{m}_n - \mathbf{m}_{prior})\right), \quad (4)$$

where $\mu_n \leq 1$ defines the step-size of the update, and $\mathbf{G}$ is a matrix containing the partial derivatives of the forward model with respect to the model parameters (i.e. the local linearisation of the problem): $(\mathbf{G}_n)^i_\alpha = (\partial g^i / \partial m^\alpha))_{m_n}$. This matrix was calculated using forward finite differences.

After finding the most likely posterior estimate using the quasi-Newton method presented

above, it is also possible to estimate the posterior covariance matrix $\tilde{\mathbf{C}}_M$, using:

$$\tilde{\mathbf{C}}_M \simeq \mathbf{C}_M - \mathbf{C}_M\mathbf{G}^T(\mathbf{G}\mathbf{C}_M\mathbf{G}^T + \mathbf{C}_D)^{-1}\mathbf{G}\mathbf{C}_M. \tag{5}$$

A second method was used for the inverse modelling step to verify the results from the least-squares solution. A Markov Chain Monte Carlo (MCMC) method was used to explore the parameter space which best matches the measurements and the given prior model parameters. The posterior of the model parameters is explored by using a random walk, where steps in the direction of likely parameter values have a higher probability of being accepted by making use of Metropolis-Hastings algorithm. This method does not rely on linearisation of the problem and is able to handle non-Gaussian assumptions on model parameters and measurement uncertainties. The MCMC method was implemented using the `PyMC3` package in python[9]. The same prior is used for the MCMC method as for the least-squares approach. Results comparing the MCMC method to the least-squares approach are presented in the next section, see Figure S3.

In Table S1 the different parameters tuned in the inverse modelling process are presented. The lower and upper values for the prior were defined as 3 times the standard deviation. An extra parameter not discussed in the text is the kernel density estimation bandwidth (KDE_{bw}). Lower and upper estimates for this parameters were set by hand, by seeing whether the predicted field for the plastic concentrations was not overly noisy or overly smoothed out. The parameter $river_{low-high}$ corresponds to the parameter representing the riverine input from Lebreton et al.[10] in terms of the lower, mid, and upper estimate as explained in the main text.

S4: Parameter estimation sensitivity study

Figure S3 presents the sensitivity study done for various tracer diffusivity values K, and different time thresholds at which particles are deleted. As explained in the main text, three

Table S1: Parameters optimized in this paper, possible values, and lower/upper bounds used in the inverse modelling process. For parameters denoted by a power of 10, the inverse modelling process was done on the exponent, in order to be able to cover a wide range of scales. Values displayed using ± indicate one times the standard deviation.

Parameter	Prior, lower estimate	Prior, upper estimate	notes
τ_{beach} [days]	10^{1}	10^{3}	See drifter buoy analysis
τ_{sink} [weeks]	$10^{0.30}$	$10^{1.72}$	Corresponds to 2–52 weeks
r_{sink} [days]	3	15	
$P_{sink,0}$ [-]	0.17	0.44	
$river_{low-high}$ [-]	-1	1	Lower to higher riverine input estimate from Lebreton et al.[10]
$S_{pop:riv}$ [-]	$10^{-1.3}$	$10^{1.3}$	Maximum contribution each source: 95%
$S_{fis:riv}$ [-]	$10^{-1.3}$	$10^{1.3}$	See above
KDE_{bw} [-]	0.05	0.2	

different values for K were studied: $K = 1$ m^2/s, $K = 10$ m^2/s, and $K = 100$ m^2/s, of which $K = 10$ m^2/s is likely the most appropriate value, given e.g. the relation used in Neumann et al.[11]:

$$K = K_0 \cdot (l/l_0)^{\frac{4}{3}}, \tag{6}$$

where K_0 is set to 1 m^2/s, l is the local grid resolution ($1/16°$, or approximately 7 km in our case), and l_0 is set to 1 km.

Most differences are observed when selecting a high tracer diffusivity of $K = 100$ m^2/s. A higher diffusivity leads to less particles remaining close to the coastal zone in the model. The beaching time scale remains relatively similar, which leads to a reduction in the sinking time scale in order to keep the right mass balance in the basin. For all simulations all source importance ratios S are relatively equal, except from $S_{fis:riv}$ for $K = 100$ m^2/s. There is an increase in the Kernel Density Estimate bandwidth (KDE_{bw}) when the tracer diffusivity increases. Possibly this could mean that a lower tracer diffusivity leads to a more realistic simulation, as results with a higher diffusivity are more smoothed out to reach a better agreement with the measured plastic concentrations.

Little differences are observed between the simulation where no particles are deleted, the simulation where particles are removed after 300 days, and where particles are removed after 180 days, all at $K = 10$ m^2/s. In order for the mass balance to hold, it was calculated that after about 50 days, 99.9% of the mass input is gone from the surface water. Keeping track of all particle trajectories indefinitely is therefore not necessary, and induces a lot of computational costs. Instead, by deleting the particles after a certain amount of time, a lot more particles can be released for less computational effort. This is important in an inverse modelling study, as multiple model iterations are necessary to converge to the right parameter estimate.

Results from the Markov Chain Monte Carlo (MCMC) analysis are consistent with the results found using the least-squares approach. Since the parameter $river_{low-high}$ converged consistently to the lower bound for the least-squares analysis, it was fixed to -1. For the rest of the parameters, minimal differences are found for the most likely MCMC values compared to the least-squares analysis for $K = 10$ m^2/s and removal at 180 days. Values in order of appearance in Figure S3 (left to right, top to bottom) for the MCMC and least-squares analysis respectively are: 24 days (24 days), 80 days (81 days), 63 days (67 days), 0.38 (0.36), 2.2 (1.9), 0.2 (0.2), 0.32 (0.31).

A summary of the total input of plastics and where plastics end up, for different tracer diffusivity values is presented in Table S2. As explained before, the higher tracer diffusivity leads to less particles remaining close to the coast, and hence less particles ending up on coastlines. Differences are quite minimal between $K = 1$ m^2/s and $K = 10$ m^2/s. The total input of plastics is relatively similar for all three tracer diffusivity values, as there is not much difference in the source importance ratios. Finally, the cost function value resulting from the inverse modelling process is presented. Although the mismatch is slightly lower for $K = 1$ m^2/s, the difference is too little to prefer this tracer diffusivity value over the others from this result alone.

Figure S4 presents the sensitivity study when adjusting the specified confidence interval

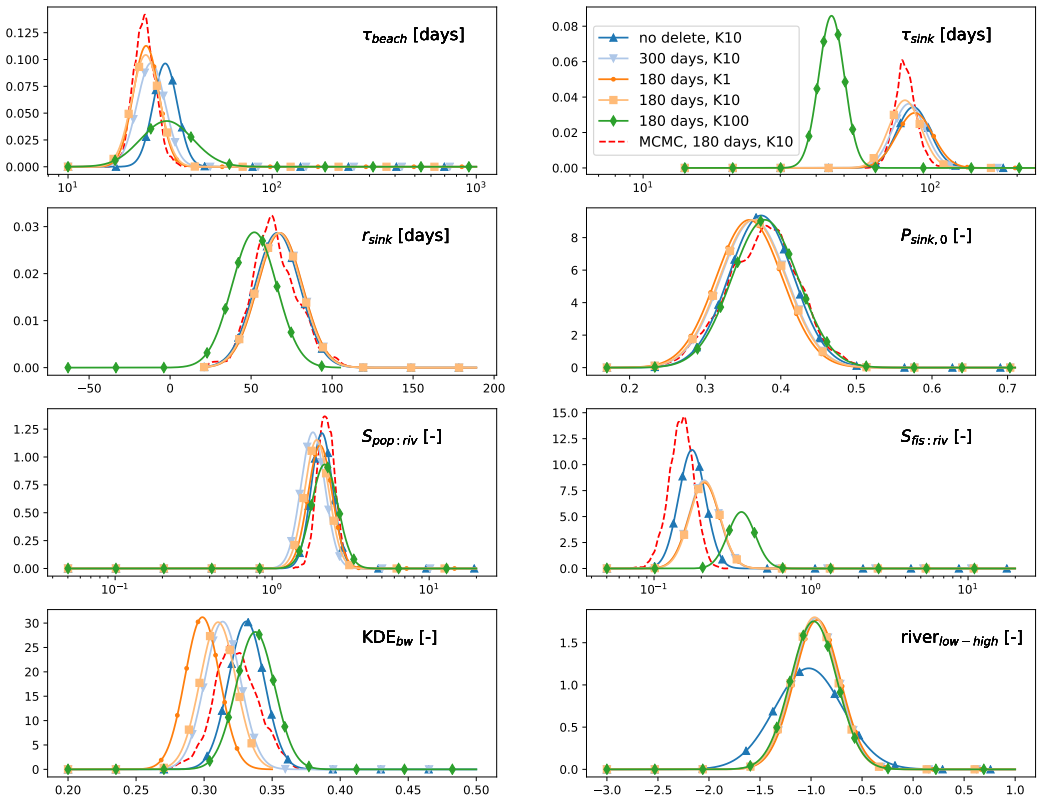

Figure S3: Sensitivity study: days until deletion and K, and the MCMC analysis

Table S2: Sensitivity study tracer diffusivity, input and sinks presented for 2006–2016 in terms of percentages and metric tonnes

Tracer diffusivity	Beaching	Sinking	Total input	Cost function value
$K = 1$ m^2/s	56%, 14,300 tonnes	43%, 11,000 tonnes	25,500 tonnes	1253
$K = 10$ m^2/s	54%, 13,800 tonnes	45%, 11,500 tonnes	25,600 tonnes	1255
$K = 100$ m^2/s	33%, 9,400 tonnes	67%, 19,100 tonnes	28,400 tonnes	1255

of the parameter bounds, and adjusting the specified variation of the measurements (all for $K = 10$ m^2/s, and deletion of particles after 180 days). The baseline simulation is presented, where the parameter bounds specify the 3σ confidence interval, and the variation of the measurements on a $\log_{10}$ scale is specified as $\gamma_n = 0.1376$ (measurements reported in terms of abundance), and $\gamma_m = 0.2201$ (measurements reported in terms of mass).

When changing the parameter bounds to the 2σ confidence interval, this means that less weight is given to deviations from the prior; when changing to the 4σ confidence interval more weight is given to deviations from the prior. Two sets of measurement variation levels were tested: one where $\gamma_n = \gamma_m = 0.32$, which comes from the reported coefficient of variation for abundance measurements from de Haan et al.[12], and $\gamma_n = 0.32$ and $\gamma_m = 0.75$ as calculated from data reported in de Haan et al.[12] for abundance and mass measurements separately. These measurement variation levels are larger than the one calculated here using the variogram method, which means that less weight is given to deviations of the model from measurements, hence it will have a similar effect as putting more weight on deviations from the prior (the C.I. = 4σ case). The main observed effect is that putting more weight to the prior will cause the Kernel Density Estimate bandwidth to be smaller. The initial sinking fraction $P_{sink,0}$ gets higher for the C.I. = 2σ case as well. In turn, to keep the right mass balance, the beaching time scale seems to increase. Almost no changes are observed in the sinking time scale, and minimal variations are present for the source importance ratios and the expected riverine input.

In the main text it was mentioned that there is likely not enough information in the data to say something about the parameter r_{sink}: its posterior is almost the same as the prior. To verify this, we did the same analysis, but changed the prior of r_{sink} to a much higher value (16 weeks instead of 9 weeks). Results are presented in Figure S5. As can be seen the posterior distribution of r_{sink} is still almost exactly the same as the prior distribution, further underlining our hypothesis there is no information in the data about this parameter.

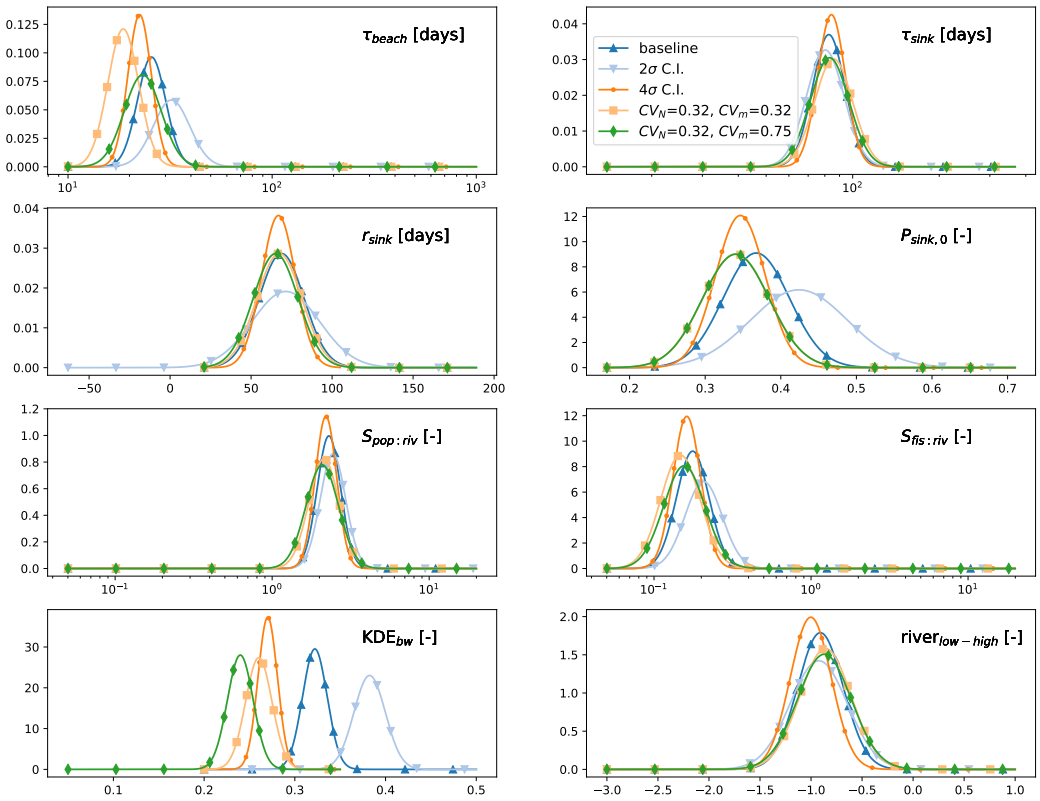

Figure S4: Sensitivity study: specified confidence interval for the prior, and coefficient of variation specified for the measurements

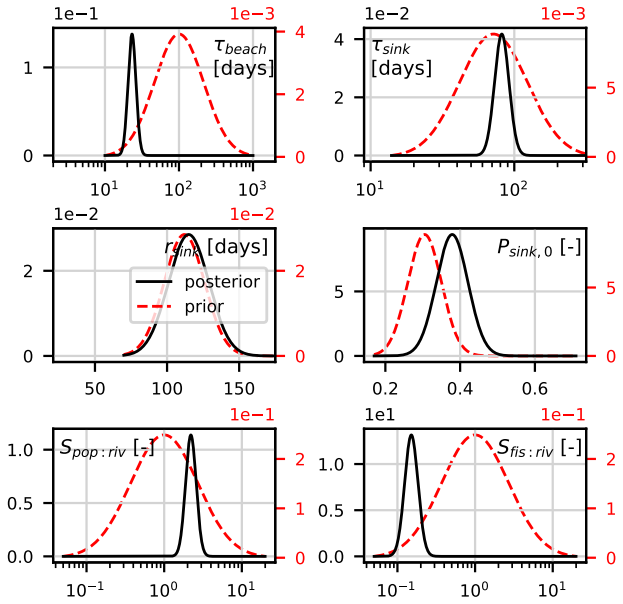

Figure S5: After changing the prior of r_{sink}, the posterior of r_{sink} is still almost exactly the same as its prior after running the inverse modelling process

S5: Model-measurement scatter plots and mass correction factor

Scatter plots showing agreement between the model and measurements (the baseline case: $K = 10$ m^2/s, deletion of particles after 180 days, $\gamma_n = 0.1376$, $\gamma_m = 0.2201$) are presented in Figure S6, for abundance measurements (left) and mass measurements (right). As can be seen, there is quite a lot of variability, and the correlation is not very high.

As discussed in the main text, variability is high due to several reasons. First of all, there is natural subgrid-scale variability which can not be captured by the model. Secondly, variance in the measurements is likely further increased due to the fact that different measurement campaigns might have slightly different measurement methodologies. The expected subgrid-scale variability was estimated in section S1 using the variogram method.

The maximum achievable correlation between the model and measurements is limited due to the high subgrid-scale variability. This is illustrated using the red solid lines in

Figure S6, which represent the model ± 2 times the standard deviation as estimated using the variogram. In case of a perfect model and accurate variability estimates, 95% of the data should lie between the red solid lines. In this case, this is 77.4% for the abundance measurements and 78.4% mass measurements. There is still room for improvement of the model, but even when 95% of the points would fall between the red lines, the maximum achievable correlation remains limited.

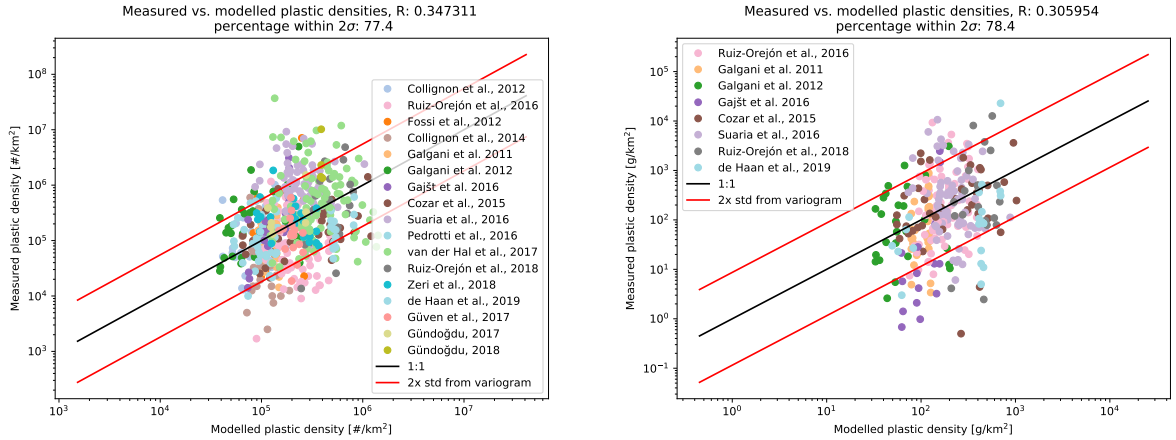

(a) Abundance (b) Mass

Figure S6: Model versus measurements: $K = 10$ m^2/s, deletion at 180 days, $\gamma_n = 0.1376$, $\gamma_m = 0.2201$

Even with high variability and low correlation, there is still information to be obtained from the observational data. In order to illustrate this, we varied the value of one parameter, τ_{sink} around its most likely posterior value (81 days) to observe what happens with the correlation and the cost function. Results are shown in Figure S7. As can be seen, the cost function value clearly attains its minimum at the most likely posterior value. The maximum correlation values are not attained at exactly the same value for τ_{sink}, but the optimization algorithm converges to a value where both are relatively high. We see however that when moving away from the most likely posterior point, there is reduction in either the correlation for the abundance concentrations or the mass concentrations.

What is also important to note, is that we are not only interested in the correlation, but also the bias of the model with respect to the measurements. By keeping the bias at

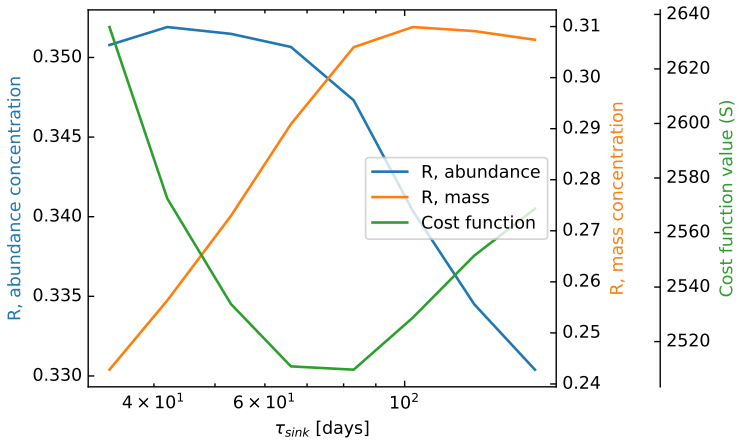

Figure S7: Effect of varying τ_{sink} around the most likely posterior value on the correlation and cost function value

a minimum, we ensure that the mass balance in the basin is consistent with the measured mass concentrations. In Figure S8 we illustrate this by choosing a too small value for τ_{sink}. Not only do we see a decreased correlation which was also illustrated in Figure S7, we also see that the model generally underpredicts the mass (most of the points now lie above the 1:1 line), leading to an incorrect mass balance.

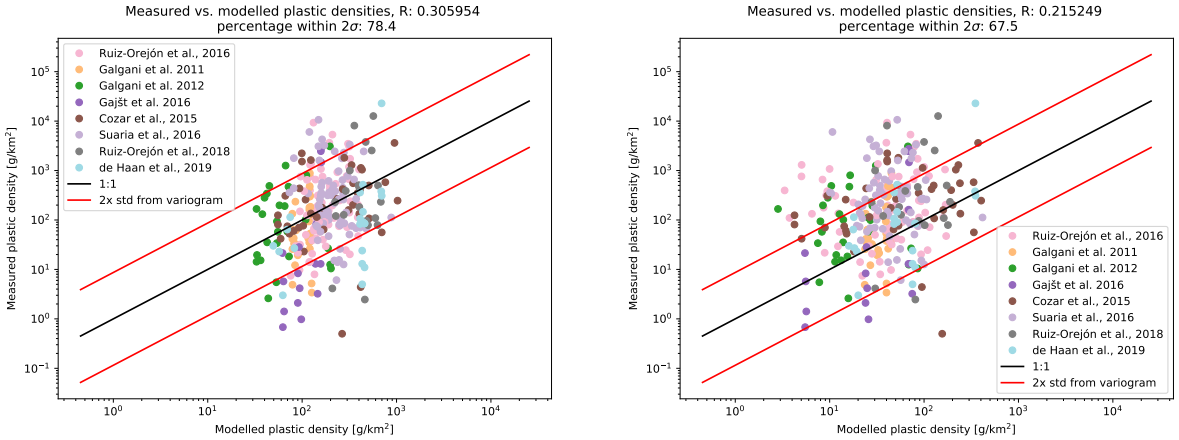

(a) τ_{sink} at the most likely posterior point

(b) At a too small τ_{sink} (12 days)

Figure S8: Moving away from the most likely posterior point not only impacts the correlation between the model and measurements negatively, it also creates a bias in the mass balance

In future work, it is recommended to look for sets of measurement campaigns with a larger

amount of data points, which are taken in a consistent manner. To illustrate this, we plotted the same scatter plots for the measurement campaign by Cózar et al. [13] only, which is the only dataset which spans both the western and the eastern Mediterranean basin. Although this is only one sample study, we do see in this case an increased correlation, and almost 90% of the data points falling within the expected 2σ bounds.

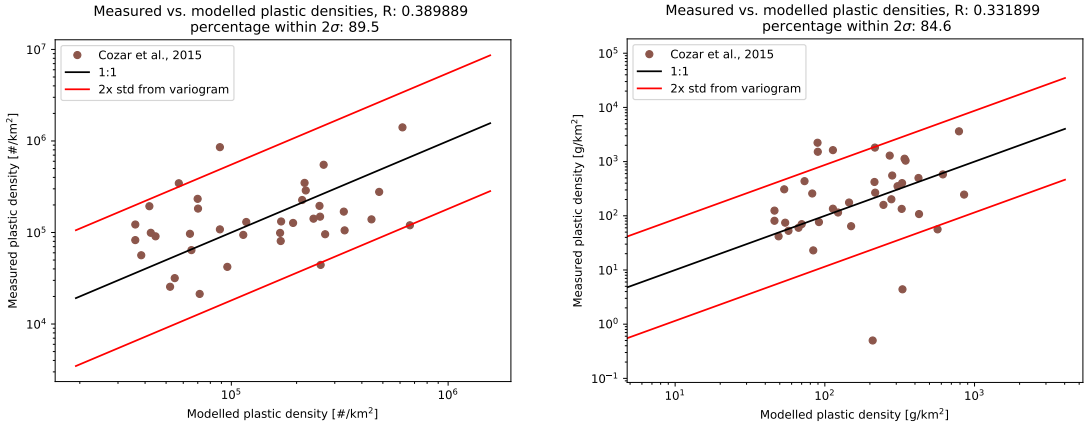

(a) Abundance (b) Mass

Figure S9: Model versus measurements: $K = 10$ m^2/s, deletion at 180 days, $\gamma_n = 0.1376$, $\gamma_m = 0.2201$ for measurements by Cózar et al. [13] only

Figure S6 also illustrates more clearly why there is an underestimation of the total floating mass in the model compared to previous estimates based on measurements only by Cózar et al. [13]. In the mass scatter plot, the model data points range from roughly 10^1 to 10^3. The measurement data points have a higher range due to their high variability, ranging from roughly 10^0 to 10^4. Since we are working on a log-log scale, the missing of the upper tails in the model distribution has a relatively high influence on the total estimated mass. A mass correction was applied, by introducing noise to the modelled plastic concentrations, where the noise is equal to the subgrid-scale variance calculated using the variogram for the mass measurements.

S6: Which sinks are neglected and why?

We will illustrate why certain sinks are neglected in this work by considering a simple mass balance model, where the floating mass inside the basin is modelled over time using

$$\frac{dm(t)}{dt} = \text{Source} - \text{Sink}. \tag{7}$$

We will consider two cases here: the *a priori* case, taking numbers from previous studies for the unknowns, and an *a posteriori* case, where we plug in our own estimates for the sources and sinks to see whether our assumptions are still valid, or whether they should be adjusted in future studies.

a priori

As *a priori* knowledge, we can use the numbers from Cózar et al.[13] where the total amount of floating plastic in the Mediterranean was estimated to be approximately 1000-3000 tonnes. Furthermore, we can use data from previous modelling studies to get an estimate on how much plastic is thought to enter the basin *a priori*: >100,000 tonnes per year.[14,15] Since the estimated input is much larger than the amount which is floating, we assume we are at least in a quasi-equilibrium, and that the estimated floating mass is approximately the steady-state value. We assume that the magnitude of the sink is dependent on the amount of floating mass: each unit of plastic mass has a certain constant probability of being removed from the surface water per unit time, defined by the sinking rate p_{sink}, from which we write:

$$\frac{dm(t)}{dt} = \text{Source} - p_{sink} \cdot m(t) = 0. \tag{8}$$

The value of p_{sink} can be related to a time scale τ by assuming a constant probability over time:

$$p_{sink} = 1 - e^{-1/\tau}. \tag{9}$$

Solving (8) for the *a priori* estimated input and estimated floating mass, yields a sinking rate p_{sink} of about 0.1 to 0.3 day^{-1}, or a time scale τ of about 3 to 10 days.

One question is whether we can neglect fragmentation in our model. In the main text it was already addressed that in Song et al. [16] weathering experiments were done, from which we can get some feeling for possible time scales. We take the volume loss of 10% for polyethylene samples subjected to 12 months of UV radiation and 2 months of mechanical abrasion, which was estimated to correspond roughly to 4 years of weathering in the environment. We can again assume this volume loss is constant over time, defined by the fragmentation rate $p_{frag.}$ (or time scale $\tau_{frag.}$). This results in a $p_{frag.}$ of about $7{\cdot}10^{-5}$ day^{-1}. We can separate the fragmentation rate from the other sinks, which will be denoted by $p_{sink,other}$ and $\tau_{sink,other}$:

$$\frac{dm(t)}{dt} = \text{Source} - p_{sink,other} \cdot m(t) - p_{frag.} \cdot m(t) = 0. \tag{10}$$

From this it is clear that $p_{sink,other}$ and $p_{frag.}$ should add up to p_{sink} in (8) in order to have a mass balance, meaning that fragmentation has no significant effect in terms of mass.

We can also analyse whether fragmentation could act as a significant source in terms of abundance, due to the production of secondary plastics. In Song et al. [16] about 20 fragments per parent particle were observed for the same scenario as described above (roughly 4 years of weathering in the environment). We write a similar balance in terms of abundance:

$$\frac{dN(t)}{dt} = \text{Source} - p_{sink,other} \cdot N(t) + p_{frag.} \cdot N(t) = 0. \tag{11}$$

We assume that the sinks have a similar influence in terms of mass as in terms of abundance: every single unit of mass, and every single plastic particle, has the same rate of being removed from the system (i.e. p_{sink} is still about 0.1 to 0.3 day^{-1}). In this case, 20 fragments over 4 years would translate to a $p_{frag.}$ of about $2{\cdot}10^{-3}$ day^{-1}. This is significantly more than the influence in terms of mass, but still two orders of magnitude lower than the magnitude of $p_{sink,other}$ that we expect.

Finally, UV radiation might convert plastic polymers into carbon dioxide and dissolved organic carbon by itself: in Ward et al.[17] the average lifetime until partial oxidation of polystyrene was estimated to range between 10 to 50 years. Assuming this process is constant over time, would lead to a UV degradation rate p_{UV} of about $3.8{\cdot}10^{-5}$ to $1.9{\cdot}10^{-4}$ day^{-1}. This is about three orders of magnitude lower than the p_{sink} required for the mass balance, and therefore neglected.

a posteriori

We can do the same analysis with the values from the mass balance obtained from the inverse modelling study. We estimated a total input of about 2,100–3,400 tonnes, and a total floating mass of 170–420 tonnes. Using these numbers, we get a required sink magnitude ranging from $p_{sink} = 1.3 \cdot 10^{-2}$ to $p_{sink} = 5.5 \cdot 10^{-2}$ day^{-1}. Using the same reasoning as above, this would mean that in terms of mass, the fragmentation rate is still expected to be significantly lower ($7{\cdot}10^{-5}$ day^{-1}, so at least two orders of magnitude) than the sinks required for the mass balance. In terms of time scales, we have τ_{sink} ranging from approximately 17 to 72 days. Removing the influence of fragmentation from the total sink would result in τ_{sink} increasing by at most 0.5%. On a similar note, considering partial oxidation of polymers (which was calculated to be $1.9{\cdot}10^{-4}$ day^{-1} for the decadal time scale reported in Ward et al.[17]), could lead to an increase in τ_{sink} of about 1.4%. Although these effects are much more important now than for the *a priori* case, it will not change the inverse modelling results dramatically.

In terms of abundance, fragmentation starts to play a bigger role, with a rate which is approximately five times lower than the lowest estimated sink magnitude ($p_{frag.} = 2 \cdot 10^{-3}$ versus $p_{sink} = 1.3 \cdot 10^{-2}$).

For a first order estimate we think that leaving out fragmentation is reasonable. Its influence was estimated to be mainly in terms of an increase in abundance. However, fragmentation will act as a net source (in terms of abundance) of secondary plastics only at the beginning of the fragmentation process. After a while a lot of the fragments will become too

small to measure (i.e. below the neuston net mesh size), leading to a net loss of particles. What is also seen in previous studies,[14,18] is that beaching patterns in generally correspond quite well with the pattern of the source itself (i.e. a majority of plastics will not travel far from its original source). This means it is likely the pattern of secondary plastic sources is quite similar to the primary sources. This likely diminishes the influence of fragmentation on the patterns of plastic concentrations in the water as modelled here. The combined effect of fragmentation as a sink for mass and a source in terms of abundance is very interesting, and is recommended to be taken in account in future studies, also because it is clear from the *a posteriori* calculations it is more important than one would think from the numbers given for the *a priori* case.

We can also turn the line of reasoning around: perhaps the discrepancy between our estimated input and the one from literature is due to neglecting fragmentation and degradation. We can take the estimated value for $p_{frag.}$ ($7{\cdot}10^{-5}$ day^{-1}) and the most conservative (largest) value for p_{UV} ($1.9{\cdot}10^{-4}$ day^{-1}), keep $p_{sink,other}$ at our *a posteriori* range ($1.3{\cdot}10^{-2}$ to $5.5{\cdot}10^{-2}$ day^{-1}), and estimate the source strength which would result in a steady-state floating mass of 170–420 tonnes. In the extreme case of taking the smallest $p_{sink,other}$ ($1.3 \cdot 10^{-2}$) and the maximum floating mass (420 tonnes) we would get a required input in the system of 8,500 tonnes. This is much higher than our estimated input (2,100 - 3,400), but one has to keep in mind that here we combined our very highest floating mass (420 tonnes), with the $p_{sink,other}$ corresponding to the very lowest input mass (2,100). These extremes correspond to the upper and lower tail of the 95% confidence interval: the probability of both occuring would be less than 0.05%. Still this increased number does not explain the difference with respect to previous studies,[14] where the input was estimated to be >100,000 tonnes per year.

References

(1) Kukulka, T.; Proskurowski, G.; Morét-Ferguson, S.; Meyer, D. W.; Law, K. L. The effect of wind mixing on the vertical distribution of buoyant plastic debris. *Geophysical Research Letters* **2012**, *39*, 1–6.

(2) Reisser, J.; Slat, B.; Noble, K.; Du Plessis, K.; Epp, M.; Proietti, M.; De Sonneville, J.; Becker, T.; Pattiaratchi, C. The vertical distribution of buoyant plastics at sea: An observational study in the North Atlantic Gyre. *Biogeosciences* **2015**, *12*, 1249–1256.

(3) Pugh, D. Tides, Surges and mean sea-level. *Marine and Petroleum Geology* **1987**, *5*, 301.

(4) Tolman, H. L.; Accensi, M.; Alves, H.; Ardhuin, F.; Bidlot, J.; Booij, N.; Bennis, A.-C.; Campbell, T.; Chalikov, D. V.; Chawla, A.; Filipot, J.-F.; Foreman, M.; Janssen, P.; Leckler, F.; Li, J.-G.; Lind, K.; Orzech, M.; Padilla-Hernandez, R.; Rogers, W. E.; Rawat, A.; Roland, A.; Sikiric, M. D.; Szyszka, M.; Tracy, B.; van Vledder, G. P. H.; van der Westhuysen, A.; Zieger, S. User manual and system documentation of WAVEWATCH III R version 4.18. **2014**,

(5) Rossby, C. G.; Montgomery, R. B. The Layer of Frictional Influence in Wind and Ocean Currents. *Papers in Physical Oceanography and Meteorology* **1935**, *3*.

(6) Menna, M.; Gerin, R.; Bussani, A.; Poulain, P.-m. *The OGS Mediterranean Drifter Dataset: 1986-2016*; 2017.

(7) Becker, J. J.; Sandwell, D. T.; Smith, W. H. F.; Braud, J.; Binder, B.; Depner, J.; Fabre, D.; Factor, J.; Ingalls, S.; Kim, S.-h.; Ladner, R.; Marks, K.; Nelson, S.; Trimmer, R.; Rosenberg, J. V.; Wallace, G.; Weatherall, P.; Trimmer, R.; Rosenberg, J. V.; Wallace, G.; Weatherall, P. Global Bathymetry and Elevation Data at 30 Arc Seconds Resolution : SRTM30 _ PLUS Global Bathymetry and Elevation Data at 30 Arc Seconds Resolution : SRTM30 PLUS. *Marine Geodesy* **2009**, *32*, 355–371.

(8) Tarantola, A. *Inverse Problem Theory and Methods for Model Parameter Estimation*; SIAM, 2005.

(9) Salvatier, J.; Wiecki, T. V.; Fonnesbeck, C. Probabilistic programming in Python using PyMC3. *PeerJ Computer Science* **2016**, *2*, e55.

(10) Lebreton, L. C.; Van Der Zwet, J.; Damsteeg, J. W.; Slat, B.; Andrady, A.; Reisser, J. River plastic emissions to the world's oceans. *Nature Communications* **2017**, *8*, 1–10.

(11) Neumann, D.; Callies, U.; Matthies, M. Marine litter ensemble transport simulations in the southern North Sea. *Marine Pollution Bulletin* **2014**, *86*, 219–228.

(12) de Haan, W. P.; Sanchez-Vidal, A.; Canals, M. Floating microplastics and aggregate formation in the Western Mediterranean Sea. *Marine Pollution Bulletin* **2019**, *140*, 523–535.

(13) Cózar, A.; Sanz-Martín, M.; Martí, E.; González-Gordillo, J. I.; Ubeda, B.; Á.gálvez, J.; Irigoien, X.; Duarte, C. M. Plastic accumulation in the mediterranean sea. *PLoS ONE* **2015**, *10*, 1–12.

(14) Liubartseva, S.; Coppini, G.; Lecci, R.; Clementi, E. Tracking plastics in the Mediterranean : 2D Lagrangian model. *Marine Pollution Bulletin* **2018**, *129*, 151–162.

(15) Jambeck, J. R.; Geyer, R.; Wilcox, C.; Siegler, T. R.; Perryman, M.; Andrady, A.; Narayan, R.; Law, K. L. Plastic waste inputs from land into the ocean. *Science* **2015**, *347*, 768–771.

(16) Song, Y. K.; Hong, S. H.; Jang, M.; Han, G. M.; Jung, S. W.; Shim, W. J. Combined Effects of UV Exposure Duration and Mechanical Abrasion on Microplastic Fragmentation by Polymer Type. *Environmental Science and Technology* **2017**, *51*, 4368–4376.

(17) Ward, C. P.; Armstrong, C. J.; Walsh, A. N.; Jackson, J. H.; Reddy, C. M. Sunlight

Converts Polystyrene to Carbon Dioxide and Dissolved Organic Carbon. *Environmental Science and Technology Letters* **2019**, *6*, 669–674.

(18) Onink, V.; Laufkötter, C. Modelling the Global Distribution of Beaching of Marine Plastic. Proceedings of the 2nd International Conference on Microplastic Pollution in the Mediterranean Sea. 2020; pp 299–305.